





## SC10X/U: A high-density electrode system for standardised surface recording of neural activity of the cervical spinal cord

Prabhav Mehra<sup>a,g,\*</sup> , Marjorie Metzger<sup>a</sup>, Saroj Bista<sup>a</sup> , Eileen R. Giglia<sup>a</sup> , Serena Plaitano<sup>a</sup>, Leah Nash<sup>a</sup>, Éanna Mac Domhnaill<sup>a</sup>, Matthew Mitchell<sup>a</sup>, Ali Khatabi<sup>i</sup>, Peter Bede<sup>b,c</sup>, Madeleine Lowery<sup>f</sup>, Muthuraman Muthuraman<sup>d,h</sup>, Orla Hardiman<sup>a,e</sup>, Bahman Nasserolelami<sup>a,g</sup> 

<sup>a</sup> Academic Unit of Neurology, School of Medicine, Trinity College Dublin, Dublin, Ireland

<sup>b</sup> Computational Neuroimaging Group, School of Medicine, Trinity College Dublin, Ireland

<sup>c</sup> Department of Neurology, St James's Hospital Dublin, Ireland

<sup>d</sup> Neural Engineering with Signal Analytics and Artificial Intelligence (NESA-AI), Universitätsklinikum Würzburg, Department of Neurology Germany

<sup>e</sup> Beaumont Hospital, Dublin, Ireland

<sup>f</sup> School of Electrical and Electronic Engineering, University College Dublin, Ireland

<sup>g</sup> SFI Future Neuro Research Centre, Trinity College Dublin, Ireland

<sup>h</sup> Informatics for Medical Technology, Institute of Computer Science, University of Augsburg, Germany

<sup>i</sup> School of Psychology, University of Birmingham, Birmingham, United Kingdom

### ARTICLE INFO

#### Keywords:

Electrospinography

SC10X/U

Spinal Cord

HD-ESG

Median nerve stimulation

10/10 EEG electrode system

### ABSTRACT

**Objective:** To develop a high-density electrode system that defines the locations of surface electrodes to record neural activity of the human cervical spinal cord; standardizing high-density electrospinography (HD-ESG) recording methodology.

**Methodology:** An electrode placement system (SC10X/U) was designed to divide the electrode space over the cervical and upper thoracic spinal cord, inspired by 10/10 EEG system. As proof of concept, a 64-channel system derived from SC10X/U was utilised to record the spinal evoked potentials in response to median nerve stimulation in ten healthy participants.

**Results:** SC10-X/U defines 76 surface electrode positions relative to anatomical references. It features a unique 10/10 system-compatible nomenclature for the locations. SC10X/U-derived HD-ESG system successfully recorded evoked spinal responses. Significant N13 and P9 potentials were observed. A post-stimulation latency of  $13.2 \pm 1.1$  ms was observed for N13 spinal-potential. Topographic map of the N13 potential indicated an epicentre at C5-C7 dorsal-vertebral levels.

**Conclusion:** The system defines electrode locations to promote standardized recordings across individuals and research centres. The evoked potentials recorded using the system conformed to the existing neurophysiological and neuroanatomical literature.

**Significance:** The proposed system addresses the gap of non-standardized multi-channel recording of neural signals from the upper spinal cord, facilitating reliable and reproducible recordings.

### 1. Introduction

The spinal cord is an integral part of the sensorimotor nervous system and plays a crucial role in the neural communication between the cortical/sub-cortical regions and periphery, which is underpinned by complex neural circuits within the spinal cord (Pierrot-Deseilligny and

Burke, 2012). These neural circuits are responsible for transmitting and processing sensorimotor signals and for establishing functional connections (Hochman, 2007). Although the SC plays an essential role in communication within sensorimotor networks, neurophysiology and neuroimaging studies have largely treated it as a wire that relays information between the brain and the periphery, ignoring the neural

\* Corresponding author at: Academic Unit of Neurology, School of Medicine, Trinity College Dublin, Dublin, Ireland.

E-mail address: [mehrap@tcd.ie](mailto:mehrap@tcd.ie) (P. Mehra).

<https://doi.org/10.1016/j.clinph.2025.2110824>

Accepted 23 June 2025

Available online 28 June 2025

1388-2457/© 2025 The Authors. Published by Elsevier B.V. on behalf of International Federation of Clinical Neurophysiology. This is an open access article under the CC BY license (<http://creativecommons.org/licenses/by/4.0/>).

complexity of the spinal cord. Similarly, neuro-electric imaging studies on sensorimotor communication have primarily focused on brain-muscle communication using Electroencephalography (EEG) – Electromyography (EMG) based analysis (Bao et al., 2021; Bista et al., 2023; Boonstra, 2013; Coffey et al., 2021; Conway et al., 1995); hence limiting our understanding of the neuro-electrophysiology of the role of the spinal cord.

Non-invasive recording of spinal neural activity is necessary to assess and analyse the function and dysfunction of spinal cord in neurodegenerative diseases (e.g. Amyotrophic Lateral Sclerosis, ALS), other neurological conditions (such as stroke), as well as across different physiological conditions in the healthy population at large. The use of spinal functional magnetic resonance imaging (fMRI) in spinal cord assessment is limited due to the structure and location of the spinal cord (Bede et al., 2012; Bede and Hardiman, 2014; Cohen-Adad, 2017). Non-invasive neuroelectric and neuro-electromagnetic imaging techniques provide high temporal resolution that is necessary for assessing spinal cord function, communication, and fast neural oscillations (Bankim Subhash Chander et al., 2022; Pierrot-Deseilligny and Burke, 2012).

In earlier electrophysiological studies, the function of the spinal cord was assessed by recording evoked potentials at lower cervical vertebral levels in response to electrical stimulation (Cioni and Meglio, 1986; Desmedt and Huy, 1984; Fujimoto et al., 2001; Prestor et al., 1997; Shimoji et al., 1971). More specifically, both invasive (Ertekin, 1976; Insola et al., 2008; Jeanmonod et al., 1991; Kaneko et al., 1998; Prestor and Golob, 1999) and non-invasive (Emerson et al., 1984; Restuccia and Mauguère, 1991; Schabrun et al., 2012; Zanette et al., 1995) recording methodologies were used to record somatosensory evoked potentials (SEPs) at spinal level in response to peripheral nerve stimulation to either understand spinal (dys)function or develop clinical biomarkers. Non-invasive short latency cervical spinal SEP's at C6 vertebrae (Cv6) level were reported at average latencies of 9 ms (P9), 11 ms (N11), and 13 ms (N13) from the posterior region (Cruccu et al., 2008; Mauguère, 2003). The N13 potentials are proposed to be generated by post-synaptic signalling in the dorsal horn of the spinal cord (Desmedt and Cheron, 1981; Jeanmonod et al., 1989; Urasaki et al., 1990). The N13 potential is considered to be the surface-level representation of the N1 potential observed in the P1-N1-P2 triphasic response via invasive epidural recording at the cervical spinal (Cioni and Meglio, 1986; Ertekin, 1976; Shimoji et al., 1971).

The earlier electrophysiological studies have primarily relied only on a limited number of channels to record the spinal activity from surface or from epidural sites. In the early 1980 s, ring electrode placement system (Desmedt and Huy, 1984; Emerson et al., 1984; Restuccia and Mauguère, 1991) was proposed to record spatial spinal evoked activity at a pre-selected cervical vertebral level. The ring electrode placement standardized the system for recording both posterior and anterior spinal activity from a particular cervical vertebra. This system still remains an active standard to record the neuro-electric activity from a select lower cervical level that has been used in more recent studies (Bankim Subhash Chander et al., 2022).

Advancements in technology have increased our capability to record neural activity from a large number of channels as observed by the increase in spatial resolution of high-density (HD) EEG and EMG recordings. Similarly, multi-channel non-invasive recording of spinal activity have become more common to increase the spatial resolution. Recent studies of HD-Magnetospinography (MSG) (Akaza et al., 2020; Mardell et al., 2024; Sumiya et al., 2017) and “multi-channel Electrospinography (ESG)” (Nierula et al., 2024) exploited multiple electrodes to record spinal activity, with the number of electrodes ranging from 16 to 44. Despite the rise of multi-channel spinal studies, there is no standardized electrode placement system for localizing the electrode space with respect to the spinal space. The absence of a recognized electrode placement standard has resulted in considerable variation in electrode locations across studies (Akaza et al., 2020; Mardell et al., 2024; Nierula et al., 2024).

In the late 1950 s, the need for a standardized electrode location for EEG recordings was recognized, and the 10–20 electrode system was proposed by Jasper, HH. (Jasper, 1958). This later advanced to the 10–10 (Chatrian et al., 1985) and 10–5 system (Oostenveld and Praamstra, 2001) as the resolution of EEG recording increased (Jurcak et al., 2007). We believe that high-density ESG will substantially benefit from a similar recognized placement system: a standardized electrode placement system that allows for compatible, comparable, and reproducible methods across research groups, participant groups, and clinicians. Moreover, this would promote standard practices that can be combined across large-scale neurophysiological and clinical studies on neurological conditions.

In this paper, we propose a high-density electrode placement system for non-invasive recording of neuroelectric signals from cervical and upper thoracic spinal cord. The proposed electrode placement system (SC10-X/U) can incorporate up to 76 channels aimed at standardizing electrode space with respect to the spinal space. This system was realised using a flexible patch for holding the electrodes. The utility of the SC10-X/U placement system is demonstrated by recording and analysing the evoked spinal potentials in response to median nerve stimulation from a 64-channel HD-ESG montage derived from the proposed SC10X/U system.

## 2. The SC10-X/U electrode system

There is currently no recognized standard electrode placement system for recording electrical activity over the cervical and upper thoracic spinal cord. The proposed SC10-X/U is described in this section, following the statement of the design requirements and criteria. The SC10-X/U system can incorporate up to 76 channel electrodes for non-invasively recording spinal activity.

We used the basic principles of the EEG 10–10 system and implemented it in the spinal cord space to design a high-density ESG electrode placement system, based on the rationale that the underlying principles of the electrode placement system defined for the brain can also be applied to the spinal cord. The principles include defining a 2D representation of the region of interest (e.g., brain, spinal cord), finding reference anatomical landmarks, and dividing the 2D space in proportional distances. In the EEG 10–10 system the 2D space is represented as a circle; anatomical references include nasion,inion, left and right preauricular points (LPA and RPA); and the space is divided into 10 % proportional distances. These principles are extended to the spinal space, resulting in the electrode placement for spinal space. The electrode placement system is named SC10X/U system.

### 2.1. The design criteria and principles of ESG electrode placement

1. *Two-dimensional representation of the space:* The cervical-thoracic spinal space can be envisioned as two curved cylinders joined together. The cervical curvature (lordotic) and the thoracic curvature (kyphotic) can be characterized as concave and convex respectively, as shown in Fig. 1. The 2D representation of the curved surface of the cylinders is described by a rectangle with curved top and bottom
2. *Anatomical Landmarks:* A total of 16 anatomical references for representing cervical and upper thoracic spinal space were selected. These include the occipital protrusion, C2 spinous process, cervical (C5 and C6) and thoracic (T1) spinous processes, left and right preauricular points, transverse spinous process of atlas (left and right), carotid tubercles (left and right), root of scapula (left and right), intersection of transverse plane through T5 spinous process and sagittal plane passing through inferior angle of scapula (left and right). These anatomical points encompass the cervical and upper thoracic spinal space as shown in Fig. 2
3. *Division of 2D space:* The medial-transverse space is divided into 10 equal segments each accounting for 10 % of the total lateral-

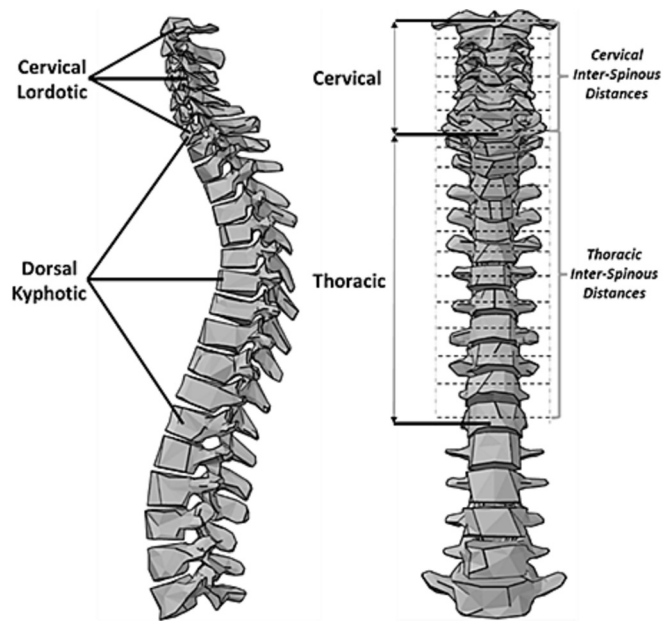


Fig. 1. Spinal Cord CAD model of the cervical and thoracic regions. The left figure shows lordotic and kyphotic curvatures of the spinal cord. The right figure represents inter-vertebral spinous distances.

medial–lateral distance, Fig. 3. The medial-sagittal space along the length and direction of the spinal cord is divided in proportion to the inter-vertebrae spinous distances contained in the electrode space (Fig. 1) shows the inter-vertebral spinous distances). The medial sagittal space encompassing the cervical spine region is divided in proportion to the average cervical intervertebral spinous distance relative to the total medial sagittal distance. Similarly, the space that encompasses the thoracic region is divided in proportion to the average thoracic intervertebral spinous distance relative to the total medial sagittal distance. The division of medial sagittal and transverse space is highlighted in Fig. 3.

2.2. SC10-X/U electrode labels: Nomenclature

The labels used in the SC10-X/U nomenclature for the electrode locations are defined by two uppercase letters followed by a number, as shown in Fig. 4. The numbering system of electrode locations follows EEG convention where the locations on the left are odd-numbered and the locations on the right are even-numbered. The nomenclature of two uppercase letters is adopted to differentiate SC10-X/U labels from EEG system labels that use single uppercase letter (optionally followed by a lowercase letter) to identify the electrode location. The label letters for the electrode positions (SC10-X/U) are defined based on the virtual vertical lines (Fig. 3) dividing the electrode space, symmetrically on either side of the spinal cord. The electrodes are sequentially numbered for each line. Sequences of odd numbers for lines that reside on the left side, sequence of even numbers for lines that reside on the right side, and sequence of 11 consecutive numbers (ML1-ML11) for lines that reside in the centre.

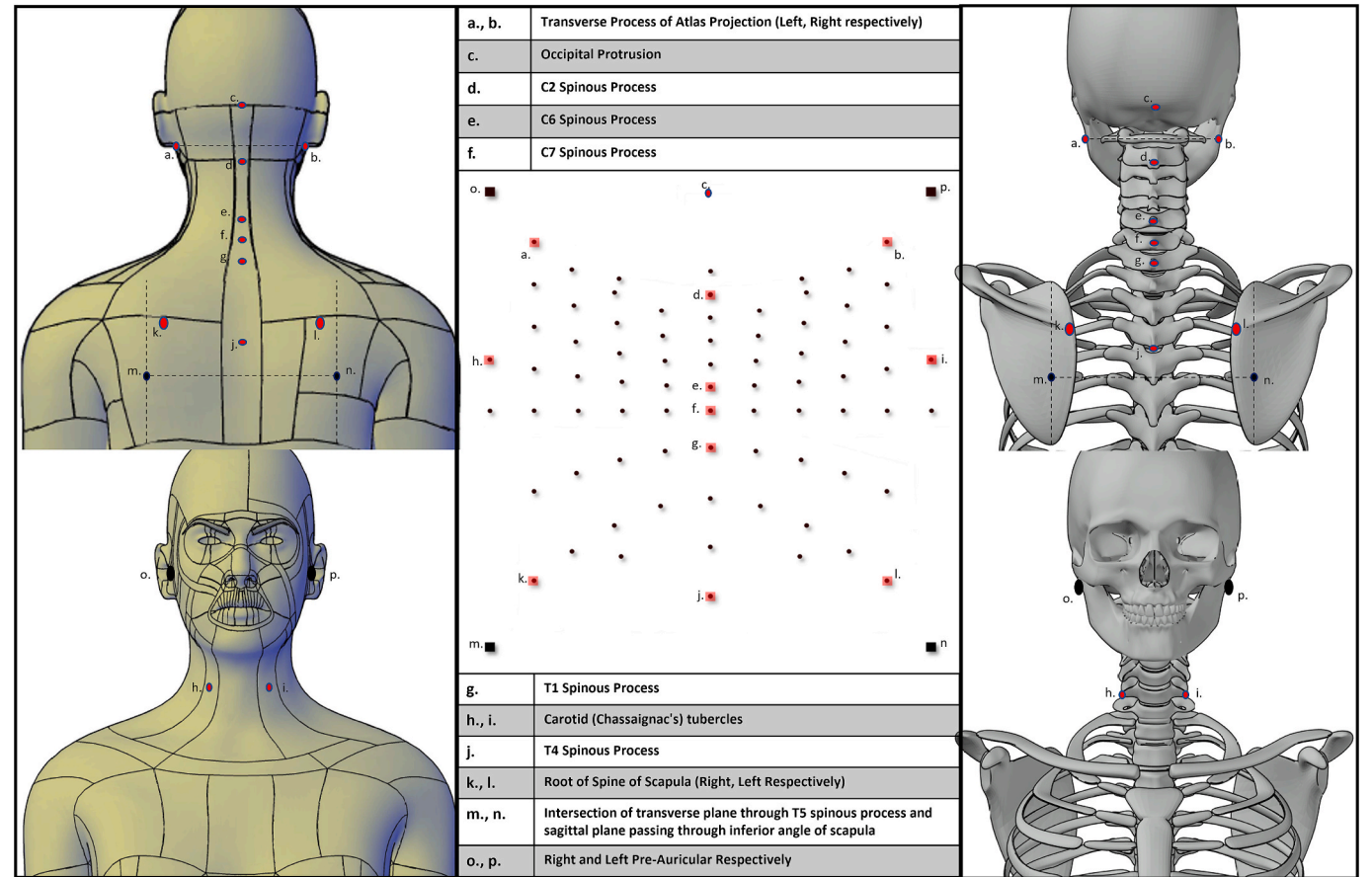


Fig. 2. Anatomical References selected as surface landmarks are shown on the human model, skeleton model, and the SC10-X/U Electrode Placement System. The anatomical points encompassing spinal space are labelled from a. to p. and are shown over the surface for the human model (left), skeleton model (right), and electrode system (centre).

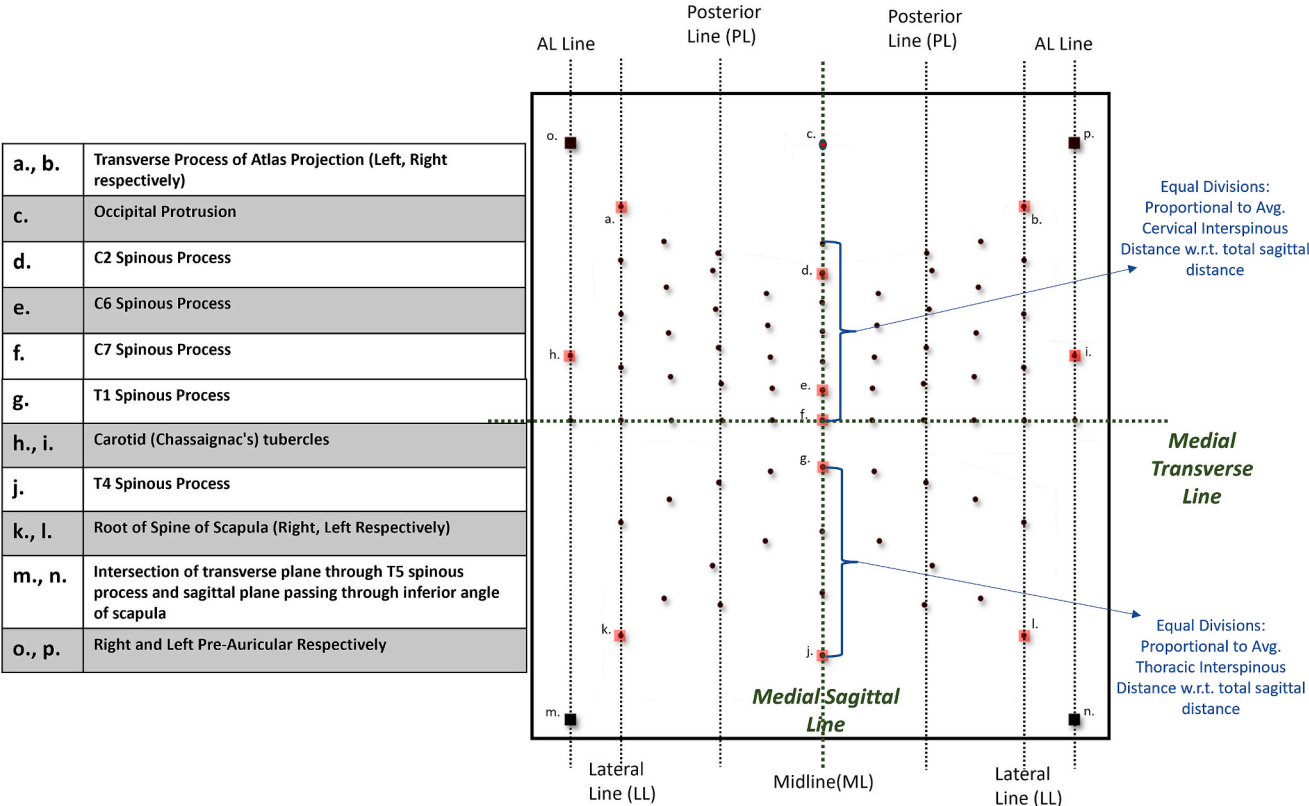


Fig. 3. Electrode placement system (SC10-X/U) representing spinal space for high-density surface electrospineography (HD-ESG). The SC10-X/U system for the 76-electrode locations is shown along with anatomical reference points and spatial features, which are utilized for 2D space division.

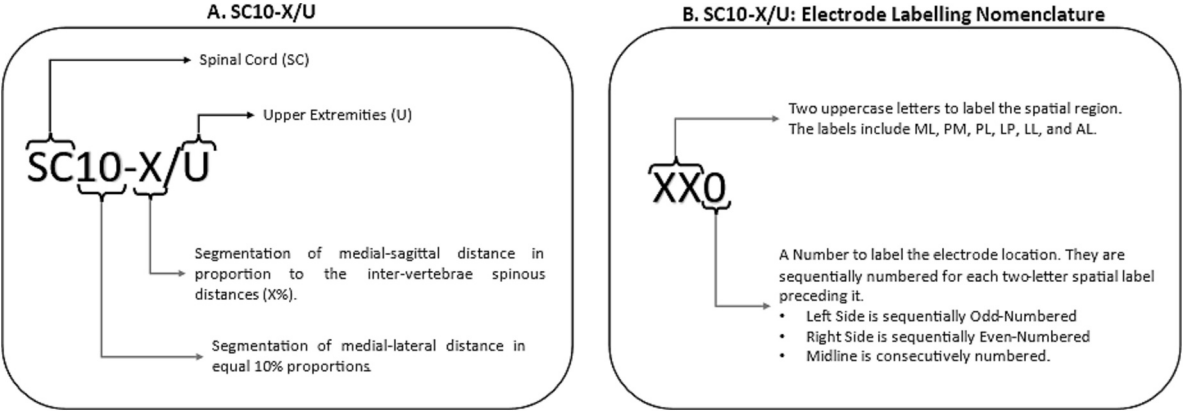


Fig. 4. A. The SC10-X/U electrode placement system acronym. B. The SC10-X/U electrode location labelling nomenclature.

The line that traces the anatomical midline of the spinal cord is defined as the Midline (ML) and encompasses the reference spinous processes; the label ML is used for the electrode locations on the midline. The virtual line named the posterior line (PL) is defined by the electrode locations that divide the transverse curves in half on either side; the label PL is used for the electrode locations on the posterior line. The virtual line that is defined along the left and right boundary of the inner-perimeter contour is referred to as the Lateral Line (LL); hence, the label LL is used for the electrode locations on the lateral line. The label PM is used for the locations that reside between the posterior line and midline and label LP is used for the locations that reside between the lateral line and posterior line. The LP and PM labels are defined by the combination of the letters from adjacent lines, where the first letter signifies the adjacent lateral line, and the second letter is defined by the adjacent medial line. Finally, the label AL is used to define the electrode

locations that rest on the AL and are in the region of the C6 anterior tubercles.

2.3. Design and Characterisation of the SC10-X/U electrode placement system

The electrode placement system shown in Fig. 3 is designed to cover the cervical and upper thoracic spinal cord space for surface neuro-electro-physiological recordings. The boundary of the space is based upon the anatomical reference points to standardize the electrode placement system. The upper boundary points are defined by the right pre-auricular and left pre-auricular points (LPA and RPA). The bottom boundary points of thoracic region are defined by the intersection of transverse plane at T5 spinous level and sagittal planes passing through the inferior angle of scapula (marked as m. and n., Fig. 2). The lateral

end points of the cervical region are defined by left and right C6 anterior tubercles (marked as h. and i., Fig. 2). The boundary is thereby defined by connecting the marked boundary points as shown in Fig. 5.a. The transverse plane passing through the C7 spinous process is divided in 10 % proportional segments (ten equidistance points) between left and right lateral ends as shown in Fig. 3 and Fig. 5.

A line is subsequently drawn along the C2, C7, T1, and T4 spinous processes to define the Midline (ML). The midline running along the spinal cord is divided into ten segments resulting in electrode positions labelled ML1 to ML11 (Fig. 5.a). The inter-electrode distance between cervical midline electrodes (ML1-ML7) and upper thoracic midline electrodes (ML8-ML11) is in proportion to the average cervical inter-vertebral spinous distances and average thoracic inter-vertebral spinous distances relative to the total medial-sagittal distance (refer to Fig. 3 and Fig. 1). The midline between ML1 and ML7 spanning cervical vertebrae levels are divided in equal proportions corresponding to the average cervical inter-spinous distance. Similarly, ML8 and ML11 spanning upper thoracic vertebral levels are divided in equal proportions corresponding to the average thoracic inter-spinous distance (Fig. 5.a). As a result, the defined electrode positions (ML1-ML11) along the midline roughly align with their respective vertebral levels.

Furthermore, the outer perimeter contour is defined by connecting LPA, RPA, ML1, ML11 position markers and AL lines (defined by connecting pre-auricular points, m., n., and C6 anterior tubercles on either side), encompassing the complete electrode space. The electrode positions one level below ML1, one level above ML11, and one level beside RPA and LPA on the lateral plane are marked as ML2, ML10, LL1, and LL2 respectively. This defines the inner-perimeter contour (Fig. 5.a). The electrodes LL1 and LL2 reside at the level of the transverse process of the atlas (marked as a. and b., Fig. 2). The left and right lines of the inner-perimeter contour are defined as Lateral Lines (LL). The Lateral Line

(LL) on the either side of contour is divided into six segments, four equal segments on cervical side and two equal segments on the thoracic side. The top and bottom segment of the left contour connecting LL1 to ML2 and LL13 to ML10 respectively are divided in two halves each. Similar divisions are made on the right top and bottom segment connecting LL2 to ML2 and LL14 to ML10. This division result in ten divisions on each half of the inner- perimeter contour. The division of inner- perimeter contour define the electrode position markers, labelled LL1, PL1, ML2, PL2, LL2, LL4, LL6, LL8, LL10, LL12, LL14, PL18, ML10, PL17, LL13, LL11, LL9, LL7, LL5, and LL3 as shown in Fig. 5.b.

Finally, a transverse curve is defined by connecting LL1 to LL2 and passing through the midline at ML3 (LL1-ML3-LL2). The defined transverse curve is divided in 8 equal fractions, resulting in positions marked by LP1, PL3, PM1, PM2, PL4, and LP2 as shown in Fig. 5.b. This is achieved by bisecting the curve twice on either side of the midline, dividing it into halves and quarters. Similar transverse curves are determined along the electrode markers LL3-ML4-LL4, LL5-ML5-LL6, LL7-ML6-LL8, LL9-ML7-LL10, LL11-ML8-LL12, and LL13-ML10-LL14 positions. These transverse curves are similarly divided in 1/8 fractions to define the remaining electrode position markers.

These steps define the resultant SC10-X/U electrode placement system (Fig. 5b) covering the spinal space encompassing the cervical and upper thoracic spinal cord.

#### 2.4. Implementation of SC10-X/U using an elastic electrode patch

An in-house non-invasive data recording elastic electrode patch was developed to realise the SC10-X/U electrode placement system. The electrode patch is designed to record spinal electrophysiological signals over spinal space covering cervical (neck) and upper thoracic (upper back) region up to T4 level. The designed elastic electrode patch can

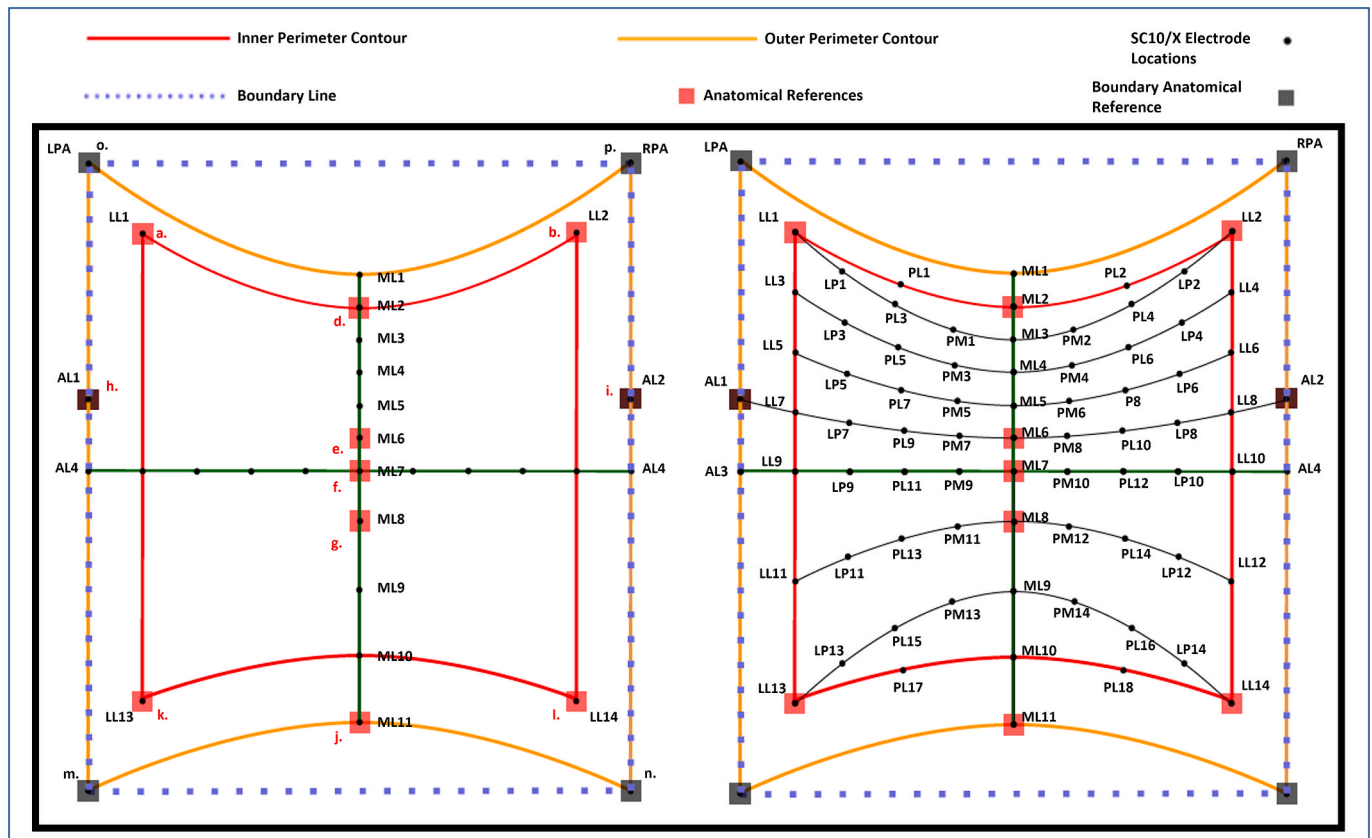


Fig. 5. Design description of the SC10-X/U electrode placement system with electrode locations and labels (right). The left figure showcases the reference boundary, inner and outer perimeter contour. The right figure showcases all 76-electrode locations and labels. The labels are defined as, ML: Midline, PM: Posterior Midline, PL: Posterior Line, LP: Lateral Posterior, LL: Lateral Line, AL: Anterior Line.

hold up to 76-channel electrodes for recording high-density Electrospinography (ESG). Here, the term ‘electrode placement system’ refers to the proposed SC10X/U system, and the term ‘electrode patch’ refers to the physical realisation of the SC10X/U standardised electrode array used for data recording.

The electrode patch was realized in six sizes to incorporate the anthropometric (inter-individual) spinal cord length variability. The average inter-cervical spinous distance for each electrode patch is determined based upon the study by Ernst, M. J., et al. (Ernst et al., 2019); average inter thoracic spinous distance is based upon an earlier study (Ernst et al., 2013). The electrode patch was developed to offer: flexibility to accommodate for curvature around neck, shoulder, and back; vertical, and horizontal stretchability to accommodate inter-individual height and width variability; and comfort for long recording sessions.

The developed electrode patch is shown in Fig. 6a. The extended lateral fins are used to hold the patch firmly against the neck (corresponding to the C4-C7 cervical spinal cord) using fasteners. The top part of the patch is held firmly against the participant with fastenings around the head. Elastic suspenders are used to hold the electrode patch around the ear and against the upper back (corresponding to the thoracic spinal cord). Fig. 6b shows the electrode patch placed over the spinal cord of a participant.

### 3. Experimental demonstration of HD-ESG: Methodology

#### 3.1. Participant and Ethics

Healthy participants ( $n = 10$ , age:  $28 \pm 4$ , 4 Males) were recruited. The experiment protocol was explained to the participants and an informed consent (signed) was taken before the recording. Ethical approval was obtained from Tallaght Hospital/St. James's Hospital Joint Research Ethics Committee for St. James's Hospital, Dublin, Ireland (Project Reference: 0493).

#### 3.2. Participant exclusion criteria

The exclusion criteria for this study include:

- (i) History of neuromuscular, neurological, or active psychiatric disease.
- (ii) Diagnosis of chronic cervical back pain or any other neck or upper back muscle stiffness, wear, and tear.
- (iii) Recent history of severe backpain, suffering with spondylosis or spondylitis or any other severe back pain / spinal degeneration.

#### 3.3. Experimental design

The experimental part of the study was aimed at observing spinal potentials recorded using HD-ESG in response to peripheral stimulation via median nerve stimulation. In addition to HD-ESG, multi-channel Electrocardiogram (ECG) signals were also acquired for removing ECG artifact from the recorded ESG signals.

During the experiment, the participants were instructed to lean forward and sit comfortably in an inclined position on the physio-chair as shown in Fig. 7b. In this position, the legs formed approximately a 60-degree angle at the knee, and the chest rest was positioned at roughly 30 degrees from the vertical plane. Throughout the recording session, the participant's head rested on the chair's headrest, and their hand was placed on the handrest, forming a 90-degree angle at the elbow. Participants were instructed to keep their eyes closed during the experiment.

The experiment consisted of a single session of median nerve stimulation, lasting approximately 20 mins. Each session consisted of 35 blocks, each block lasted for 30 s and consisted of 20 s of stimulation followed by 10 s of rest. In the stimulation phase, a train of stimulation pulses at an average frequency of 2 Hz were applied at the wrist of the right hand to elicit stimulation of the median nerve. Stimulation was applied using a constant current stimulator DS7A (Digitimer Ltd., UK). DS7A is MDD CE medically certified and can provide up to 100 mA

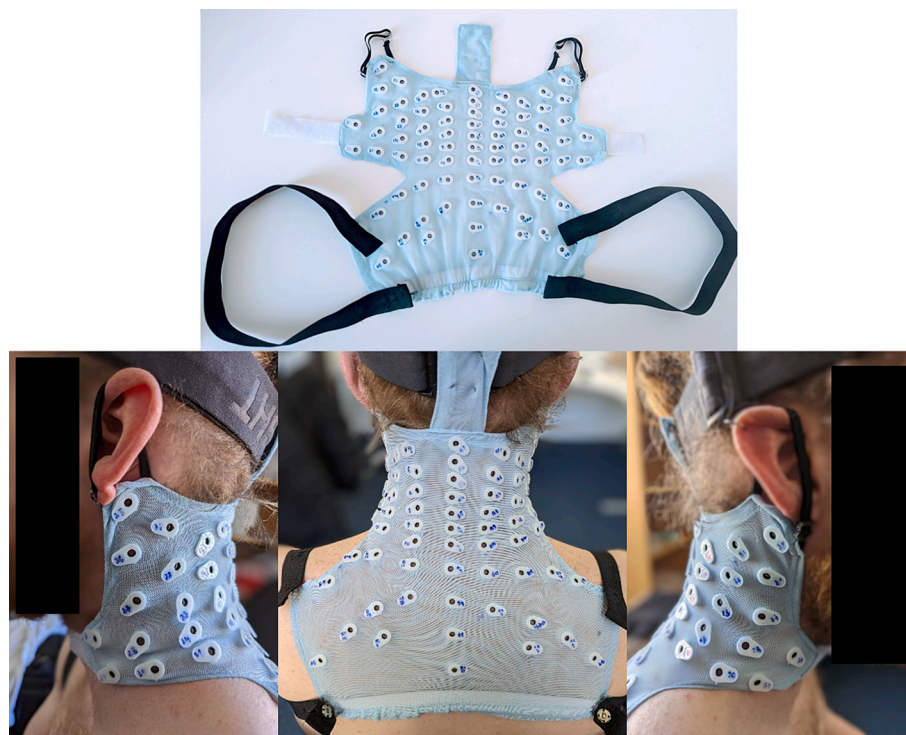


**Fig. 6.** a. In-house developed electrode patch based upon the SC10-X/U electrode system. b. The electrode patch (up to 76 electrode channels) placed over the surface of the cervical and upper thoracic spinal cord space of an individual.

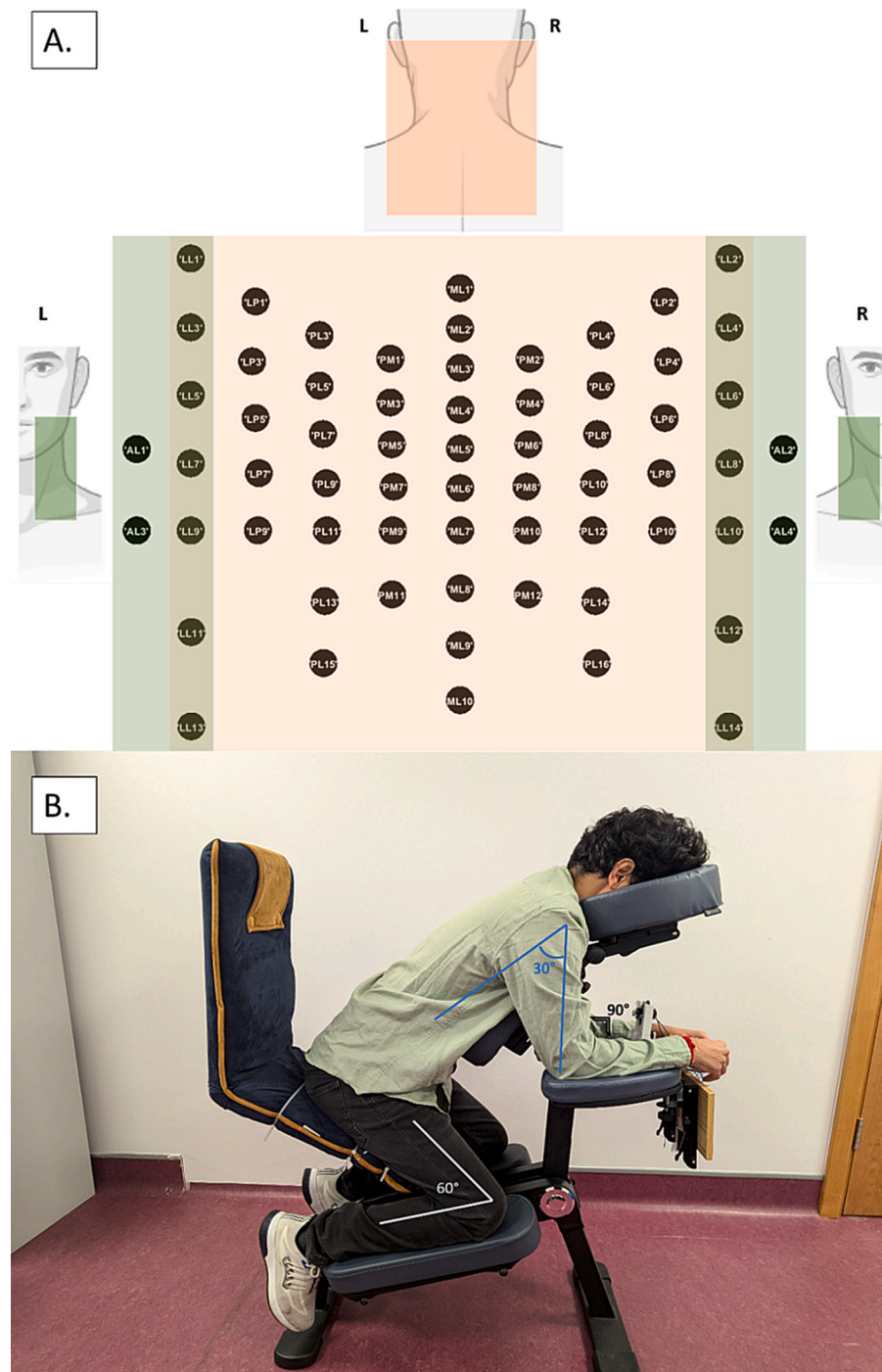


**Fig. 7.** A. The 64-electrode channels used for the recording and its corresponding electrode space. B. A demonstrator sitting in an inclined position on the physio-chair. The demonstrator's chest was supported by the chest rest while their head rested on the headrest and hands rested on the handrest respectively.

constant current high voltage pulses. The stimulation intensity was set to 1.5 times the motor threshold and the pulse width was set to 200  $\mu$ s. The motor threshold was defined as the minimum intensity at which consistent prominent thumb movement were observed. In the session, a total of 1400 trial responses (35 block x 40 stimulations per block) to peripheral stimulation were recorded.

### 3.4. Data acquisition

The data collection system consisted of a high-density biosignal amplifier that was used for high density ESG, and multi-channel ECG. The Electrical Activity of 64 (ESG) + 5 (ECG) + 8 (EXG) channels were

recorded simultaneously using the high-speed Biosemi-ActiveTwo system (Biosemi B.V., Amsterdam, The Netherlands) at a sampling frequency of 8 kHz, with a bandpass filter over 0 Hz – 1600 Hz frequency range. All electrode channels were visually inspected for signal quality prior to recording and the electrode offset was kept between  $\pm 25$  mV.

The HD-ESG signals were recorded using 64-channel active electrodes with placement following the SC10-X/U electrode system. The 64-channel ESG montage was derived from the proposed system (Fig. 7a). The active electrodes were connected to the electrode holder of the electrode patch and electrolyte paste was used to enhance skin-electrode connection.

Multi-channel ECG was recorded in accordance with the 5-electrode

ECG system with flat active sintered Ag-AgCl electrodes. The following 7-lead ECG signals were extracted from the 5-electrode ECG system:

1.  $Lead I = LA - RA$
2.  $Lead II = LL - RA$
3.  $Lead III = LL - LA$
4.  $aVR = RA - \frac{1}{2}(LA + LL)$
5.  $aVL = LA - \frac{1}{2}(RA + LL)$
6.  $aVF = LL - \frac{1}{2}(RA + LA)$
7.  $Lead V1 = V1 - \frac{1}{3}(RA + LA + LL)$

Eight additional signals were collected using flat active sintered Ag-AgCl electrodes. The electrodes were placed at the following locations: (i) left and right earlobe, (ii) to the left of the left eye and to the right of the right eye, (iii) left and right clavicle, (iv) below left eye, (v) erb's point (brachial plexus).

### 3.5. Data analysis

The signals were analysed using MATLAB (The MathWorks, 2023) scripts in conjunction with the FieldTrip toolbox (Oostenveld et al., 2011) and the NoiseTool toolbox (de Cheveigné et al., 2018).

### 3.6. Signal pre-processing

Two main contaminating artifacts were identified in the recorded ESG signals: stimulation and ECG artifacts. The stimulation artifact lasted approximately 1–2 ms; this artifact was identified and the signal during this period was interpolated using piecewise cubic interpolation. ECG artifact in the ESG signal were removed by applying canonical correlation analysis (CCA) (de Cheveigné et al., 2018; Hotelling, 1936). This was achieved by isolating and removing the two canonical components that represented the highest correlation between ESG data (64 channels) and ECG leads (7 leads). The first two canonical components (CC) were selected for removal, as the correlation (r) score after the first two CCs demonstrated a sharp decrease in magnitude.

The remaining CCs were back-transformed to the original space to provide the denoised ESG signal. The signal post artifact rejection was re-referenced using 'common average referencing'. The re-referenced signals were baseline corrected and segmented into epochs of 0.5 s, starting 0.1 s before the stimulation and ending 0.4 s after the stimulation. Before further processing of the signal, bad channels were visually determined and interpolated (weighted average) based on the signal from neighbouring channels (neighbour distance  $\leq 50$  mm). The epoched trials were visually inspected and the bad trials were rejected. The remaining trials ( $1287 \pm 91$  trials,  $\sim 92\%$ ) were bandpass filtered between 10 and 1500 Hz (Insola et al., 2008; Prestor et al., 1997), dual-pass Butterworth filter.

### 3.7. Event-Locked activity

The pre-processed epochs from the ESG channels underwent event-locked analysis. The epochs were averaged over all the good trials. Surface Laplacian referencing, based on Hjorth's method (Carvalhaes and de Barros, 2015; Hjorth, 1975) was applied to the averaged signals. The resulting signals were analyzed to identify characteristics of the event-locked (time-phase locked) evoked activity and spatial distribution of the evoked activity.

### 3.8. Statistical analysis

A statistically significant difference from zero of the evoked activity was identified at each time from all participants, using the Wilcoxon signed-rank non-parametric test (Iyer et al., 2017; Nasserolelami et al.,

2014). To account for multiple comparisons in 64 channels and several time points ( $-0.001$  s –  $0.03$  s), we retained the dominant 4 principal components that explained 85 % of the total variance, plus an additional component ( $4 + 1 = 5$ ). Bonferroni correction was subsequently applied at  $\alpha = 0.05$ .

## 4. Demonstration of HD-electrospinography: Results

High-density electrospinography (HD-ESG) using non-invasive 64-channel surface electrodes was used to record spinal activity in response to median nerve stimulation. The event-locked activity was evaluated for the recorded signals.

### 4.1. Average evoked potential

The average (across trials) evoked potential for individual participants and the grand-mean signal across participants at channel ML6 (C6 vertebral level) are shown in Fig. 8 (respectively in grey and black). Significant evoked potentials P9 and N13 were recorded at ML6 (C6 cervical level); marked in red in Fig. 8. The observed latency of the evoked potential N13 and P9 across individual participants was  $13.2 \pm 1.1$  ms (mean  $\pm$  sd) and  $9.7 \pm 1.2$  ms (mean  $\pm$  sd) respectively.

Electrode channels AL1, LL7, LP7, PL9, PM7, ML6, PM8, PL8, LP8, LL8, and AL2 from the SC10-X/U system are comparable to the traditional ring electrode placement at the C6 vertebral level traditionally used to record spinal evoked potential in response to median nerve stimulation (Restuccia and Manguière, 1991). The grand mean signal across participants for the channels used to define the ring electrodes system is shown in Fig. 9. In Fig. 9, the evoked potential at 13 ms has the highest amplitude at channel ML6 and reverses polarity at the anterior-lateral electrode channel (AL2).

### 4.2. Topographic map of evoked spinal potentials

High density spinal activity recorded using the SC10X/U electrode placement system was used to map the spatial distribution of the electrical activity across the spinal space. The topographical plot of grand-mean spinal evoked response during the time frame 12–14 ms (N13) after the median nerve stimulation is shown in Fig. 10. The region around the midline indicates higher spinal response activity with its epicentre at channels ML4-ML6. Another epicentre of spinal response with reversed polarity is also indicated in Fig. 10 at the lower cervical right-anterior-lateral and right-lateral regions.

The grand-mean response of the midline electrodes in the cervical region (ML2-ML7) can also be seen in Fig. 10. The lower cervical level channels on the right side of the Topography map (Fig. 10) indicate reversed polarity of the evoked potentials in the region.

## 5. Discussion

This study proposes an HD electrode placement system (SC10-X/U) for recording the electrophysiology activity of the cervical spinal cord. The utility of the proposed SC10X system was demonstrated by recording evoked spinal activity (HD-ESG) in response to median nerve stimulation with high spatial resolution. The SC10X/U system promotes a standardised methodology for recording high-density ESG signals at the cervical and upper thoracic spinal levels. This addresses the technical gap leading to non-standardized multichannel neurophysiological recordings being utilized by recent studies for estimating spinal signals in response to external stimulation (Akaza et al., 2020; Mardell et al., 2024; Sumiya et al., 2017) or for developing spatial filters to access single trial spinal evoked potentials (Nierula et al., 2024). These studies indicate the potential benefits of high-density spinographic techniques over non-HD recordings but fail to facilitate compatible and reproducible research across individuals and research groups. The proposed system maps the cervical and upper thoracic region to the electrode

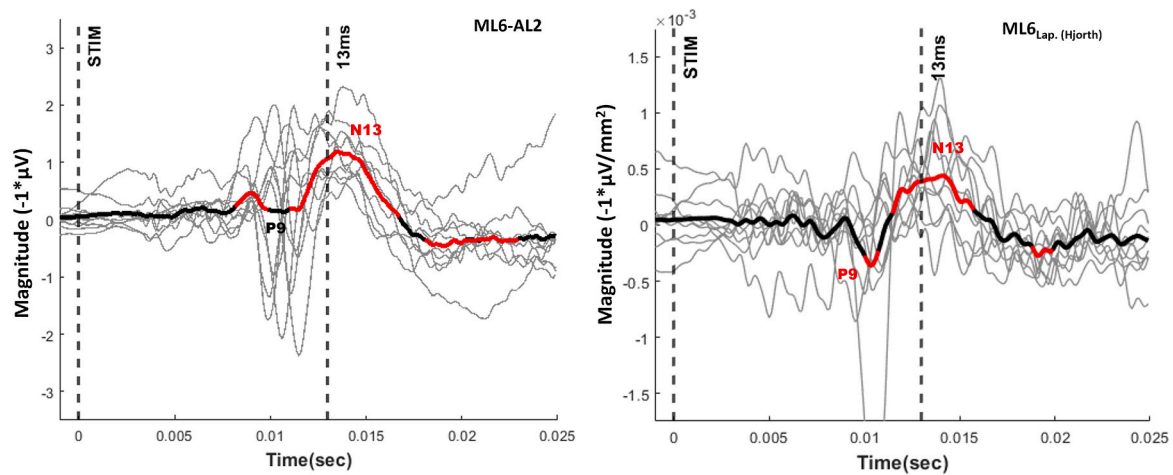


**Fig. 8.** Grand-mean of the evoked potentials across all participants at ML6 electrode. Grey lines represent individual participant evoked potentials, and thick black line correspond to the grand mean evoked potential across all participants. The duration of significant evoked response ( $p < 0.01$ ) is highlighted by red lines. The figure indicates significant N13 and P9 evoked potentials. a. ML6 response in reference to AL2 electrode (left). b. surface Laplacian re-referenced ML6 response (right). (For interpretation of the references to colour in this figure legend, the reader is referred to the web version of this article.)

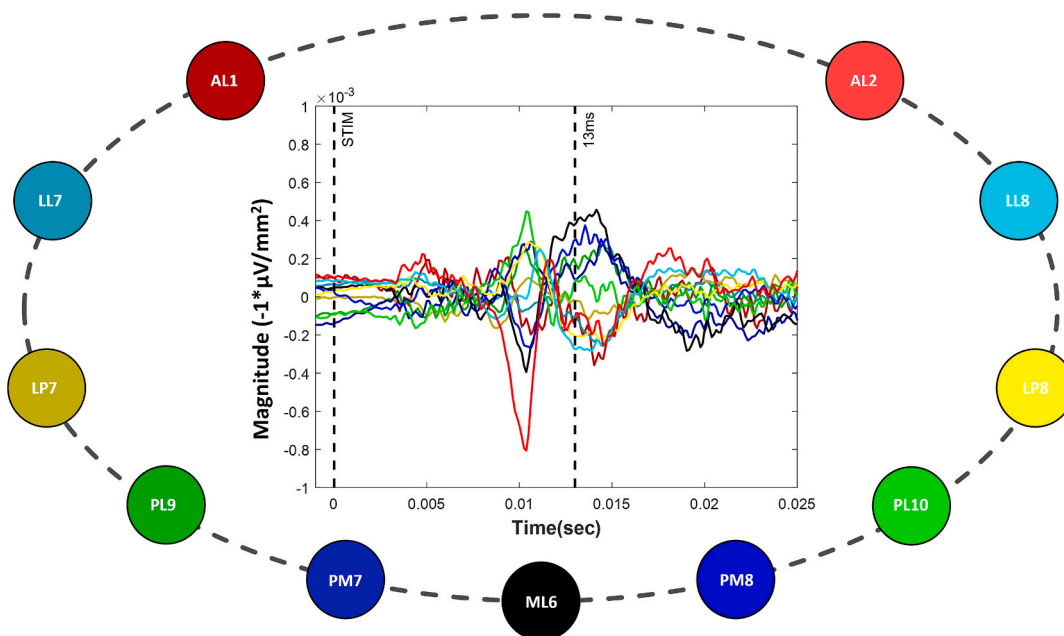


**Fig. 9.** Grand-mean signals plotted for SC10-X/U channels at Cv6 compatible with ring electrode placement system at Cv6. (Surface Laplacian re-referenced).

space for non-invasive neuroelectric imaging and can incorporate up to 76 channels as shown in Fig. 3. This is especially suitable for sensorimotor studies investigating the upper extremities.

Development of the SC10-X/U electrode placement system is aimed at the standardization of future studies, to enable compatible, comparable, and reproducible methods across individuals and research centres. EEG electrode placement systems (10/20, 10/10, 10/5) have proven to be an invaluable tool in the field of neuro-electro-physiology, enabling standardized electrophysiological recording resulting in applications including development of biomarkers (de Aguiar Neto and Rosa, 2019; McMackin et al., 2019), brain-computer interface (Lotte et al., 2007; Zhang et al., 2018), and resting-state analyses (Dukic et al., 2022; Metzger et al., 2023). Similarly, standardized high-density electrospinalography presents huge potential in uncovering the role of the spinal cord in sensorimotor processing within the central nervous system and moving away from treating SC as a “wire” relay between the brain and periphery.

The SC10-X/U system was demonstrated using a 64-channel electrode patch to record evoked spinal activity in response to the median nerve stimulation. Short latency SEP's P9, and N13 were recorded as shown in Fig. 8, and corroborate previous studies (Crucchi et al., 2008; Mauguère, 2003) with consistent SEP measures and anatomically valid location of responses that represented the corresponding dermatome (Cramer et al., 2014). Posterior cervical channels showed a negative evoked response approximately 13 ms (N13) after stimulation. The N13 potential is believed to be generated by the dorsal horn and to have a post-synaptic origin (Desmedt and Cheron, 1981; Jeanmonod et al., 1989; Urasaki et al., 1990). We also observed reversed polarity of N13 response when moving from the posterior (ML6) to right-anterior electrodes (AL2) at an approximate C6 vertebral level, as demonstrated in previous studies (Desmedt and Huy, 1984; Restuccia and Mauguère, 1991). Furthermore, the observed inter-individual variability in N13 latency was within the expected limits for a healthy population (Desmedt and Cheron, 1981; Di Pietro et al., 2021; Insola et al., 2008).

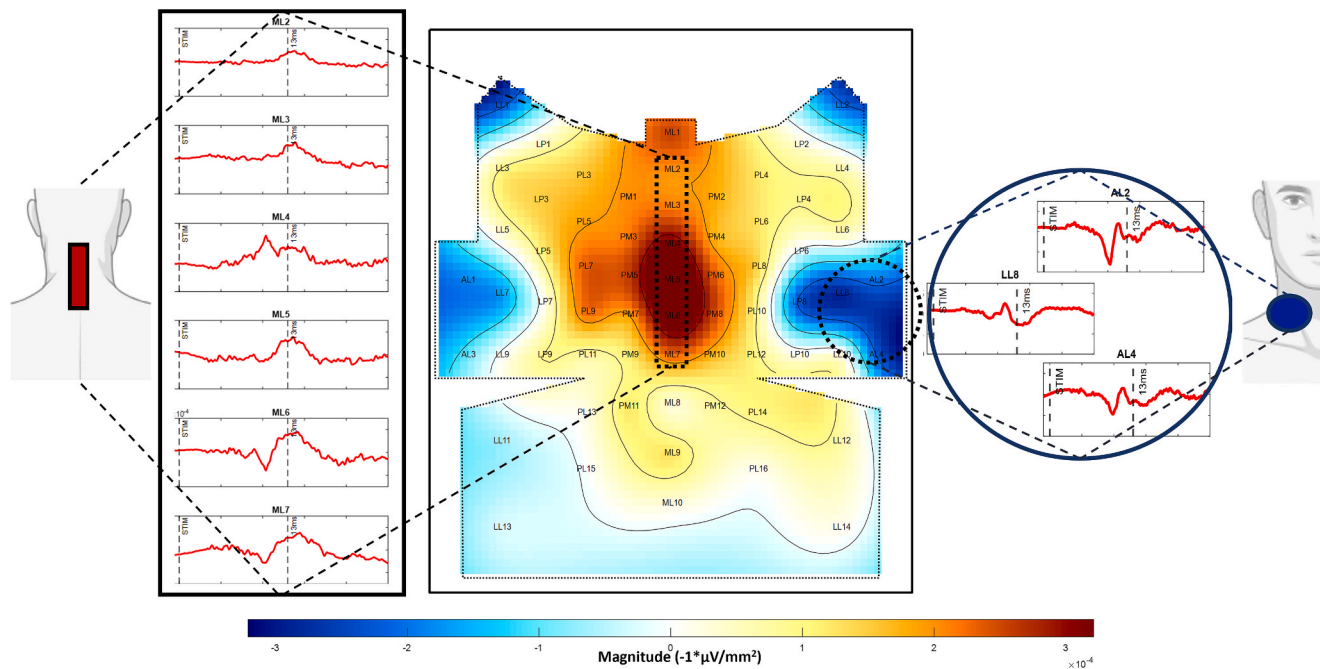


**Fig. 10.** Topographic Map of Evoked Spinal Potentials. Centre Figure: Topographic Map of the grand-mean spinal evoked response over the SC10-X/U sensor space, time-window (12 ms–14 ms). Left figure: corresponds to the spinal activity recorded from channels ML2–ML7 (midline, posterior) for the time frame between 0.001 s before stimulation and 0.025 s after stimulation. Right figure: corresponds to the spinal activity recorded from lateral-anterior channels for the time frame between 0.001 s before stimulation and 0.025 s after stimulation.

The variability can be attributed to differences in anatomical factors such as height and limb length, as well as physiological factors such as conduction velocity due to sex, age, handedness and athletic fitness (Beigi et al., 2023; Maudrich et al., 2022; Nobue and Ishikawa, 2024; Patel and Mehta, 2012; Waghmare et al., 2025).

The spatial distribution of the observed spinal activity was mapped using the HD electrode channels. The topographic map indicated that high cervical spinal activity is localized around the midline with its epicenter at ML4–ML6 level (Fig. 10). This epicentre could correspond to fibres from roots of spinal nerves C5–C7, innervation of which is contained in the median nerve. Moreover, an epicenter of high activity was also seen around the anterior and lateral region at lower cervical levels, through the polarity is reversed. The observed evoked potentials and their characteristics are compatible with the existing literature (Crucchi et al., 2008; Mauguière, 2003). The results from previous studies recorded using ring electrode placement (Restuccia and Mauguière, 1991) can be extended and interpreted using the comparable electrode locations from the proposed SC10-X/U system, i.e. electrode channels AL1, LL7, LP7, PL9, PM7, ML6, PM8, PL8, LP8, LL8, and AL2 from SC10-X/U system are comparable to the traditional ring electrode system. Here, we demonstrated in Fig. 9 that the evoked potentials recorded at the selected electrode channels are comparable to the evoked activity reported in studies using ring placement electrode system (Bankim Subhash Chander et al., 2022; Restuccia and Mauguière, 1991).

Development of the standardised HD-ESG recording system will enable advanced analysis of evoked responses using combined spatial, spectral, and temporal techniques similar to those used for HD-EEG. Standardized HD-ESG in conjunction with advanced spatial ESG filtering techniques (Bailey et al., 2024) would help extract spinal neural signals from the physiological noise, improving the signal to noise ratio. Furthermore, recording standardized HD-ESG alongside standardized EEG would enable further investigation of spinal cord dysfunction within the neural control system in neurological conditions.

The future direction of this study would be to investigate the spatiotemporal changes in the evoked HD-spinal potentials in response to peripheral nerve stimulation in neurodegenerative conditions, such as

amyotrophic lateral sclerosis, that affect sensorimotor communication.

## 6. Conclusion

The SC10-X/U electrode system described in this paper provides full coverage of the cervical and upper thoracic region by closely and evenly spaced high-density electrodes applied at standardized locations with respect to accessible anatomical locations. The system can incorporate up to 76 electrode positions, though certain studies may require only a subset of electrodes to cover the spinal space of interest. The utilization of this system in studies of spontaneous (such as resting state, task-related) and evoked ESG activity is expected to facilitate compatible and reproducible research. In theory, information derived from the surface-recorded ESG could be projected onto the anatomical space and communicated through the use of a standardized atlas across different research and participant groups, promoting the identification of sources of neural activity within the spinal cord. This should promote standard practices across large-scale neurophysiological and clinical studies of neurological conditions.

## CRedit authorship contribution statement

**Prabhav Mehra:** Conceptualization, Methodology, Writing – original draft, Writing – review & editing. **Marjorie Metzger:** Methodology, Writing – review & editing. **Saroj Bista:** Methodology, Writing – review & editing. **Eileen R. Giglia:** Writing – review & editing. **Serena Plaitano:** Writing – review & editing. **Leah Nash:** Writing – review & editing. **Éanna Mac Domhnaill:** Writing – review & editing. **Matthew Mitchell:** Project administration, Writing – review & editing. **Ali Khatibi:** Writing – review & editing. **Peter Bede:** Writing – review & editing. **Madeleine Lowery:** Writing – review & editing. **Muthuraman Muthuraman:** Writing – review & editing. **Orla Hardiman:** Writing – review & editing. **Bahman Nasseroleslami:** Conceptualization, Writing – review & editing, Supervision.

## Funding

Prabhav Mehra was supported by Provost's PhD Project Awards (to Bahman Nasserolelami), Trinity College Dublin, the University of Dublin, FHS190014. The research costs of this project was supported by Trinity College Dublin's Wellcome Trust Institutional Strategic Support Fund (ISSF), funded by the University of Dublin and Wellcome Trust. This publication has emanated from research supported in part by a research grant from Research Ireland under Grant Number 21/RC/10294\_P2 and co-funded under the European Regional Development Fund and by FutureNeuro industry partners. Peter Bede was supported by the Health Research Board (JPND-Cofund-2-2019-1 and HRB EIA-2017-019) and Science Foundation Ireland (SFI SP20/SP/8953).

## Declaration of Competing Interest

The authors declare that they have no known competing financial interests or personal relationships that could have appeared to influence the work reported in this paper.

## References

- Akaza, M., Kawabata, S., Ozaki, I., Miyano, Y., Watanabe, T., Adachi, Y., Sekihara, K., Sumi, Y., Yokota, T., 2020. Noninvasive measurement of sensory action currents in the cervical cord by magnetospinography. *Clin. Neurophysiol.* 132, 382–391. <https://doi.org/10.1016/j.clinph.2020.11.029>.
- Bailey, E., Nierula, B., Stephani, T., Maess, B., Nikulin, V., Eippert, F., 2024. Evaluating noise correction approaches for non-invasive electrophysiology of the human spinal cord. doi: 10.1101/2024.09.05.611423.
- Chander, B.S., Deliano, M., Azanón, E., Buntjen, L., Stenner, M.-P., 2022. Non-invasive recording of high-frequency signals from the human spinal cord. *Neuroimage* 253, 119050. <https://doi.org/10.1016/j.neuroimage.2022.119050>.
- Bao, S.-C., Chen, C., Yuan, K., Yang, Y., Tong, R.-K.-Y., 2021. Disrupted cortico-peripheral interactions in motor disorders. *Clin. Neurophysiol.* 132, 3136–3151. <https://doi.org/10.1016/j.clinph.2021.09.015>.
- Bede, P., Bokde, A.L.W., Byrne, S., Elamin, M., Fagan, A.J., Hardiman, O., 2012. Spinal cord markers in ALS: diagnostic and biomarker considerations. *Amyotroph. Lateral Scler.* 13, 407–415. <https://doi.org/10.1080/17482968.2011.649760>.
- Bede, P., Hardiman, O., 2014. Lessons of ALS imaging: pitfalls and future directions — a critical review. *NeuroImage Clin.* 4, 436–443. <https://doi.org/10.1016/j.nicl.2014.02.011>.
- Beigi, S., Shabkhiz, F., Kordi, M., Haghi-Ashtiani, B., Hashemi-Madani, N., Zmijewski, P., 2023. The effects of a 10-week aerobic and unilateral lower extremity resistance training program on amplitude and nerve conduction velocity of sensory and motor nerves in diabetic patients with neuropathy. *J. Hum. Kinet.* 87, 93–103. <https://doi.org/10.5114/jhk/161610>.
- Bista, S., Coffey, A., Fasano, A., Buxo, T., Mitchell, M., Giglia, E.R., Dukic, S., Heverin, M., Muthuraman, M., Carson, R.G., Lowery, M., Hardiman, O., McManus, L., Nasserolelami, B., 2023. Cortico-muscular coherence in primary lateral sclerosis reveals abnormal cortical engagement during motor function beyond primary motor areas. *Cereb. Cortex* 33, 8712–8723. <https://doi.org/10.1093/cercor/bhad152>.
- Boonstra, T., 2013. The potential of corticomuscular and intermuscular coherence for research on human motor control. *Front. Hum. Neurosci.* 7.
- Carvalhoes, C., de Barros, J.A., 2015. The surface Laplacian technique in EEG: theory and methods. *Int. J. Psychophysiol.* 97, 174–188. <https://doi.org/10.1016/j.ijpsycho.2015.04.023>.
- Chatrian, G.E., Lettich, E., Nelson, P.L., 1985. Ten percent electrode system for topographic studies of spontaneous and evoked EEG activities. *Am. J. EEG Technol.* 25, 83–92. <https://doi.org/10.1080/00029238.1985.11080163>.
- Cioni, B., Meglio, M., 1986. Epidural recordings of electrical events produced in the spinal cord by segmental, ascending and descending volleys. *Stereotact. Funct. Neurosurg.* 49, 315–326. <https://doi.org/10.1159/000100161>.
- Coffey, A., Bista, S., Fasano, A., Buxo, T., Mitchell, M., Giglia, E.R., Dukic, S., Fenech, M., Barry, M., Wade, A., Heverin, M., Muthuraman, M., Carson, R.G., Lowery, M., Hardiman, O., Nasserolelami, B., 2021. Altered supraspinal motor networks in survivors of poliomyelitis: a cortico-muscular coherence study. *Clin. Neurophysiol.* 132, 106–113. <https://doi.org/10.1016/j.clinph.2020.10.011>.
- Cohen-Adad, J., 2017. Functional magnetic RESONANCE IMAGING OF THE SPINAL CORD: CURRENT STATUS AND FUTURE DEVELOPMENTS. *Semin. Ultrasound CT MRI, Spinal Cord Imaging, Part 2* 38, 176–186. <https://doi.org/10.1053/j.sult.2016.07.007>.
- Conway, B.A., Halliday, D.M., Farmer, S.F., Shahani, U., Maas, P., Weir, A.I., Rosenberg, J.R., 1995. Synchronization between motor cortex and spinal motoneuronal pool during the performance of a maintained motor task in man. *J. Physiol.* 489, 917–924. <https://doi.org/10.1113/jphysiol.1995.sp021104>.
- Cramer, G.D., Darby, S.A., Cramer, G.D., 2014. *Clinical anatomy of the spine, spinal cord, and ANS*, 3rd ed. Elsevier, St. Louis, Mo.
- Crucchi, G., Aminoff, M.J., Curio, G., Guerit, J.-M., Kakigi, R., Mauguère, F., Rossini, P. M., Treede, R.-D., Garcia-Larrea, L., 2008. Recommendations for the clinical use of somatosensory-evoked potentials. *Clin. Neurophysiol.* 119, 1705–1719. <https://doi.org/10.1016/j.clinph.2008.03.016>.
- de Aguiar Neto, F.S., Rosa, J.L.G., 2019. Depression biomarkers using non-invasive EEG: a review. *Neurosci. Biobehav. Rev.* 105, 83–93. <https://doi.org/10.1016/j.neubiorev.2019.07.021>.
- de Cheveigné, A., Wong, D.D.E., Di Liberto, G.M., Hjortkjaer, J., Slaney, M., Lalor, E., 2018. Decoding the auditory brain with canonical component analysis. *Neuroimage* 172, 206–216. <https://doi.org/10.1016/j.neuroimage.2018.01.033>.
- Desmedt, J.E., Cheron, G., 1981. Prevertebral (oesophageal) recording of subcortical somatosensory evoked potentials in man: the spinal P13 component and the dual nature of the spinal generators. *Electroencephalogr. Clin. Neurophysiol.* 52, 257–275. [https://doi.org/10.1016/0013-4694\(81\)90055-9](https://doi.org/10.1016/0013-4694(81)90055-9).
- Desmedt, J.E., Huy, N.T., 1984. BIT-mapped colour imaging of the potential fields of propagated and segmental subcortical components of somatosensory evoked potentials in man. *Electroencephalogr. Clin. Neurophysiol.* 58, 481–497. [https://doi.org/10.1016/0013-4694\(84\)90037-3](https://doi.org/10.1016/0013-4694(84)90037-3).
- Di Pietro, G., Di Stefano, G., Leone, C., Di Lionardo, A., Sgro, E., Blockeel, A.J., Caspani, O., Garcia-Larrea, L., Mouraux, A., Phillips, K.G., Treede, R.-D., Valeriani, M., Truini, A., 2021. The N13 spinal component of somatosensory evoked potentials is modulated by heterotopic noxious conditioning stimulation suggesting an involvement of spinal wide dynamic range neurons. *Neurophysiol. Clin.* 51, 517–523. <https://doi.org/10.1016/j.neucli.2021.09.001>.
- Dukic, S., McMackin, R., Costello, E., Metzger, M., Buxo, T., Fasano, A., Chipika, R., Pinto-Grau, M., Schuster, C., Hammond, M., Heverin, M., Coffey, A., Broderick, M., Iyer, P.M., Mohr, K., Gavin, B., McLaughlin, R., Pender, N., Bede, P., Muthuraman, M., van den Berg, L.H., Hardiman, O., Nasserolelami, B., 2022. Resting-state EEG reveals four subphenotypes of amyotrophic lateral sclerosis. *Brain* 145, 621–631. <https://doi.org/10.1093/brain/awab322>.
- Emerson, R.G., Seyal, M., Pedley, T.A., 1984. Somatosensory evoked potentials following median nerve stimulation: I. The cervical components. *Brain* 107, 169–182. <https://doi.org/10.1093/brain/107.1.169>.
- Ernst, M.J., Rast, F.M., Bauer, C.M., Marcar, V.L., Kool, J., 2013. Determination of thoracic and lumbar spinal processes by their percentage position between C7 and the PSIS level. *BMC. Res. Notes* 6, 58. <https://doi.org/10.1186/1756-0500-6-58>.
- Ernst, M.J., Sommer, B.B., Meichtry, A., Bauer, C.M., 2019. Intra-rater reliability of determining positions of cervical spinous processes and measuring their relative distances. *BMC. Res. Notes* 12, 265. <https://doi.org/10.1186/s13104-019-4299-8>.
- Ertekin, C., 1976. Studies on the human evoked electrospino-gram. *Acta Neurol. Scand.* 53, 3–20. <https://doi.org/10.1111/j.1600-0404.1976.tb04321.x>.
- Fujimoto, H., Kaneko, K., Taguchi, T., Ofuji, A., Yonemura, H., Kawai, S., 2001. Differential recording of upper and lower cervical N13 responses and their contribution to scalp recorded responses in median nerve somatosensory evoked potentials. *J. Neurol. Sci.* 187, 17–26. [https://doi.org/10.1016/S0022-510X\(01\)00509-3](https://doi.org/10.1016/S0022-510X(01)00509-3).
- Hjorth, B., 1975. An on-line transformation of EEG scalp potentials into orthogonal source derivations. *Electroencephalogr. Clin. Neurophysiol.* 39, 526–530. [https://doi.org/10.1016/0013-4694\(75\)90056-5](https://doi.org/10.1016/0013-4694(75)90056-5).
- Hochman, S., 2007. Spinal cord. *Curr. Biol.* 17, R950–R955. <https://doi.org/10.1016/j.cub.2007.10.014>.
- Hotelling, H., 1936. Relations between two sets of variates. *Biometrika* 321–377.
- Insola, A., Padua, L., Mazzone, P., Valeriani, M., 2008. Unmasking of presynaptic and postsynaptic high-frequency oscillations in epidural cervical somatosensory evoked potentials during voluntary movement. *Clin. Neurophysiol.* 119, 237–245. <https://doi.org/10.1016/j.clinph.2007.09.132>.
- Iyer, P.M., Mohr, K., Broderick, M., Gavin, B., Burke, T., Bede, P., Pinto-Grau, M., Pender, N.P., McLaughlin, R., Vajda, A., Heverin, M., Lalor, E.C., Hardiman, O., Nasserolelami, B., 2017. Mismatch negativity as an indicator of cognitive sub-domain dysfunction in amyotrophic lateral sclerosis. *Front. Neurol.* 8, 395. <https://doi.org/10.3389/fneur.2017.00395>.
- Jasper, H., 1958. Ten-twenty electrode system of the international federation. *Electroencephalogr. Clin. Neurophysiol.* 10, 371–375.
- Jeanmonod, D., Sindou, M., Mauguère, F., 1989. Three transverse dipolar generators in the human cervical and lumbo-sacral dorsal horn: evidence from direct intraoperative recordings on the spinal cord surface. *Electroencephalogr. Clin. Neurophysiol. Potentials Sect.* 74, 236–240. [https://doi.org/10.1016/0013-4694\(89\)90010-2](https://doi.org/10.1016/0013-4694(89)90010-2).
- Jeanmonod, D., Sindou, M., Mauguère, F., 1991. The human cervical and lumbo-sacral evoked electrospino-gram. Data from intra-operative spinal cord surface recordings. *Electroencephalogr. Clin. Neurophysiol. Potentials Sect.* 80, 477–489. [https://doi.org/10.1016/0168-5597\(91\)90129-L](https://doi.org/10.1016/0168-5597(91)90129-L).
- Jurcak, V., Tsuzuki, D., Dan, I., 2007. 10/20, 10/10, and 10/5 systems revisited: their validity as relative head-surface-based positioning systems. *Neuroimage* 34, 1600–1611. <https://doi.org/10.1016/j.neuroimage.2006.09.024>.
- Kaneko, K., Kawai, S., Taguchi, T., Fuchigami, Y., Ito, T., Morita, H., 1998. Correlation between spinal cord compression and abnormal patterns of median nerve somatosensory evoked potentials in compressive cervical myelopathy: comparison of surface and epidurally recorded responses. *J. Neurol. Sci.* 158, 193–202. [https://doi.org/10.1016/S0022-510X\(98\)00119-1](https://doi.org/10.1016/S0022-510X(98)00119-1).
- Lotte, F., Congedo, M., Lécuyer, A., Lamarche, F., Arnaldi, B., 2007. A review of classification algorithms for EEG-based brain-computer interfaces. *J. Neural Eng.* 4, R1. <https://doi.org/10.1088/1741-2560/4/2/R01>.
- Mardell, L.C., Spedden, M.E., O'Neill, G.C., Tierney, T.M., Timms, R.C., Zich, C., Barnes, G.R., Bestmann, S., 2024. Concurrent spinal and brain imaging with optically

- pumped magnetometers. *J. Neurosci. Methods* 406, 110131. <https://doi.org/10.1016/j.jneumeth.2024.110131>.
- Maudrich, T., Hähner, S., Kenville, R., Ragert, P., 2022. Somatosensory-evoked potentials as a marker of functional neuroplasticity in athletes: a systematic review. *Front. Physiol.* 12, 821605. <https://doi.org/10.3389/fphys.2021.821605>.
- Mauguière, F., 2003. Chapter 5 Somatosensory evoked responses. In: Hallett, M. (Ed.), *Handbook of Clinical Neurophysiology, Handbook of Clinical Neurophysiology*. Elsevier, pp. 45–75. doi: 10.1016/S1567-4231(09)70153-4.
- McMackin, R., Bede, P., Pender, N., Hardiman, O., Nasserolleslami, B., 2019. Neurophysiological markers of network dysfunction in neurodegenerative diseases. *NeuroImage Clin.* 22, 101706. <https://doi.org/10.1016/j.nicl.2019.101706>.
- Metzger, M., Dukic, S., McMackin, R., Giglia, E., Mitchell, M., Bista, S., Costello, E., Peelo, C., Tadjine, Y., Sirenko, V., Plaitano, S., Coffey, A., McManus, L., Farnell Sharp, A., Mehra, P., Heverin, M., Bede, P., Muthuraman, M., Pender, N., Hardiman, O., Nasserolleslami, B., 2023. Functional network dynamics revealed by EEG microstates reflect cognitive decline in amyotrophic lateral sclerosis. *Hum. Brain Mapp.* 45, e26536. <https://doi.org/10.1002/hbm.26536>.
- Nasserolleslami, B., Lakany, H., Conway, B.A., 2014. EEG signatures of arm isometric exertions in preparation, planning and execution. *Neuroimage* 90, 1–14. <https://doi.org/10.1016/j.neuroimage.2013.12.011>.
- Nierula, B., Stephani, T., Bailey, E., Kaptan, M., Pohle, L.-M.-G., Horn, U., Mouraux, A., Maess, B., Villringer, A., Curio, G., Nikulin, V.V., Eippert, F., 2024. A multichannel electrophysiological approach to noninvasively and precisely record human spinal cord activity. *PLoS Biol.* 22, e3002828. <https://doi.org/10.1371/journal.pbio.3002828>.
- Nobue, A., Ishikawa, M., 2024. Sex-specific differences in peripheral nerve properties: a comparative analysis of conduction velocity and cross-sectional area in upper and lower limbs. *Diagnostics* 14, 2711. <https://doi.org/10.3390/diagnostics14232711>.
- Oostenveld, R., Fries, P., Maris, E., Schoffelen, J.-M., 2011. FieldTrip: open source software for advanced analysis of MEG, EEG, and invasive electrophysiological data. *Comput. Intell. Neurosci.* 1–9. <https://doi.org/10.1155/2011/156869>.
- Oostenveld, R., Praamstra, P., 2001. The @ve percent electrode system for high-resolution EEG and ERP measurements. *Clin Neurophysiol.*
- Patel, A., Mehra, A., 2012. A comparative study of nerve conduction velocity between left and right handed subjects. *Int. J. Basic Appl. Physiol.* 1, 19–21.
- Pierrot-Deseilligny, E., Burke, D., 2012. *The Circuitry of the Human Spinal Cord: Spinal and Corticospinal Mechanisms of Movement*, 1st ed. Cambridge University Press. doi: 10.1017/CBO9781139026727.
- Prestor, B., Gnidovec, B., Golob, P., 1997. Long sensory tracts (cuneate fascicle) in cervical somatosensory evoked potential after median nerve stimulation. *Electroencephalogr. Clin. Neurophysiol.* 104, 470–479. [https://doi.org/10.1016/s0168-5597\(97\)00040-3](https://doi.org/10.1016/s0168-5597(97)00040-3).
- Prestor, B., Golob, P., 1999. Intra-operative spinal cord neuromonitoring in patients operated on for intramedullary tumors and syringomyelia. *Neurol. Res.* 21, 125–129. <https://doi.org/10.1080/01616412.1999.11740908>.
- Restuccia, D., Mauguière, F., 1991. The contribution of median nerve SEPs in the functional assessment of the cervical spinal cord in syringomyelia. A study of 24 patients. *Brain* 114, 361–379. <https://doi.org/10.1093/brain/114.1.361>.
- Schabrun, S.M., Ridding, M.C., Galea, M.P., Hodges, P.W., Chipchase, L.S., 2012. Primary sensory and motor cortex excitability are co-modulated in response to peripheral electrical nerve stimulation. *PLoS One* 7, 1–7. <https://doi.org/10.1371/journal.pone.0051298>.
- Shimoji, K., Higashi, H., Kano, T., 1971. Epidural recording of spinal electrogram in man. *Electroencephalogr. Clin. Neurophysiol.* 30, 236–239. [https://doi.org/10.1016/0013-4694\(71\)90059-9](https://doi.org/10.1016/0013-4694(71)90059-9).
- Sumiya, S., Kawabata, S., Hoshino, Y., Adachi, Y., Sekihara, K., Tomizawa, S., Tomori, M., Ishii, S., Sakaki, K., Ukegawa, D., Ushio, S., Watanabe, T., Okawa, A., 2017. Magnetospinography visualizes electrophysiological activity in the cervical spinal cord. *Sci. Rep.* 7, 2192. <https://doi.org/10.1038/s41598-017-02406-8>.
- The MathWorks, I., 2023. MATLAB and Computer Vision System Toolbox.
- Urasaki, E., Wada, S.-I., Kadoya, C., Tokimura, T., Yokota, A., Matsuoka, S., Fukumura, A., Hamada, S., 1990. Skin and epidural recording of spinal somatosensory evoked potentials following median nerve stimulation: correlation between the absence of spinal N13 and impaired pain sense. *J. Neurol.* 237, 410–415. <https://doi.org/10.1007/BF00314731>.
- Waghmare, L.S., Waghmare, T.L., Ambad, R.S., 2025. Gender differences in nerve conduction parameters of upper limb nerves in healthy adults: a comparative study. *J. Pharm. Bioallied Sci.* 17, S410. <https://doi.org/10.4103/jpbs.jpbs.1811.24>.
- Zanette, G., Tinazzi, M., Manganotti, P., Bonato, C., Polo, A., 1995. Two distinct cervical N13 potentials are evoked by ulnar nerve stimulation. *Electroencephalogr. Clin. Neurophysiol. Potentials Sect.* 96, 114–120. [https://doi.org/10.1016/0168-5597\(94\)00212-W](https://doi.org/10.1016/0168-5597(94)00212-W).
- Zhang, W., Tan, C., Sun, F., Wu, H., Zhang, B., 2018. A review of EEG-Based brain-computer interface systems design. *Brain Sci. Adv.* 4, 156–167. <https://doi.org/10.26599/BSA.2018.9050010>.